

## A Surface-Aware Projection Basis for Quasigeostrophic Flow

K. SHAFER SMITH

*Center for Atmosphere Ocean Science, Courant Institute of Mathematical Sciences, New York University, New York, New York*

JACQUES VANNESTE

*School of Mathematics and Maxwell Institute for Mathematical Sciences, University of Edinburgh, Edinburgh, United Kingdom*

(Manuscript received 18 June 2012, in final form 31 October 2012)

### ABSTRACT

Recent studies indicate that altimetric observations of the ocean's mesoscale eddy field reflect the combined influence of surface buoyancy and interior potential vorticity anomalies. The former have a surface-trapped structure, while the latter are often well represented by the barotropic and first baroclinic modes. To assess the relative importance of each contribution to the signal, it is useful to project the observed field onto a set of modes that separates their influence in a natural way. However, the surface-trapped dynamics are not well represented by standard baroclinic modes; moreover, they are dependent on horizontal scale.

Here the authors derive a modal decomposition that results from the simultaneous diagonalization of the energy and a generalization of potential enstrophy that includes contributions from the surface buoyancy fields. This approach yields a family of orthonormal bases that depend on two parameters; the standard baroclinic modes are recovered in a limiting case, while other choices provide modes that represent surface and interior dynamics in an efficient way.

For constant stratification, these modes consist of symmetric and antisymmetric exponential modes that capture the surface dynamics and a series of oscillating modes that represent the interior dynamics. Motivated by the ocean, where shears are concentrated near the upper surface, the authors consider the special case of a quiescent lower surface. In this case, the interior modes are independent of wavenumber, and there is a single exponential surface mode that replaces the barotropic mode. The use and effectiveness of these modes is demonstrated by projecting the energy in a set of simulations of baroclinic turbulence.

### 1. Introduction

Because direct observations of the ocean's interior are sparse, satellite altimetry plays a crucial role in determining its time-dependent, three-dimensional velocity structure. This indirect measurement process assumes that sea surface height variations are dominated by currents with low-mode vertical structure, a result of the stiffening action of rotation and ensuing barotropization. Observations provide some support for this assumption, at least on lateral scales of order the first internal deformation scale and above. For example, using current meter records in conjunction with satellite observations, Wunsch (1997) argues that the bulk of the

ocean's eddy kinetic energy resides in the barotropic and first baroclinic modes. In addition, a number of studies show a strong correlation between the lateral size of eddies and the first internal deformation scale (e.g., Stammer 1997; Chelton et al. 2011).

However, recent theoretical developments, supported by simulation and improved analysis of satellite altimetry, suggest that surface signals are not well-correlated with low-mode vertical structure, especially for submesoscale motions. In particular, Lapeyre and Klein (2006) argue that surface buoyancy and upper-ocean potential vorticity are anticorrelated for eddying flow, and that the three-dimensional velocity field may be obtained, assuming quasigeostrophy, from knowledge of the surface buoyancy field alone. The dynamics at the upper surface in this view are closely related to the surface quasigeostrophic (SQG) model (Blumen 1982; Held et al. 1995), and imply a vertical structure with a surface-trapped component that is not well represented by standard baroclinic modes.

---

*Corresponding author address:* K. Shafer Smith, Courant Institute of Mathematical Sciences, New York University, 251 Mercer St., New York, NY 10012.  
E-mail: shafer@cims.nyu.edu

This view is supported by results from idealized simulations (LaCasce and Mahadevan 2006; Klein et al. 2008), realistic simulations (Isern-Fontanet et al. 2008), and recent analyses of satellite altimetry (e.g., Isern-Fontanet et al. 2006; Le Traon et al. 2008). Finally, in an atmospheric context, Tulloch and Smith (2009) have shown that lateral surface buoyancy gradients may interact with interior mean potential vorticity gradients to excite baroclinically unstable modes that generate SQG-like dynamics near the upper surface. In simulations, the resulting kinetic energy spectrum near the surface exhibits a steep  $-3$  slope just below the deformation scale, and a flatter  $-5/3$  slope at smaller scales—translated to the oceanic context, this implies an energetic submesoscale dominated by the surface mode.

One of the most widely used tools in oceanography is the projection of the vertical structure of observed or simulated currents on simple bases of functions. The above observations and modeling results lead one to seek projection bases that faithfully represent both the low-mode interior structure and the surface dynamics. The standard basis of baroclinic modes, consisting of the eigenfunctions  $F_n(z)$  of the eigenvalue problem

$$\begin{aligned} \frac{d}{dz} \left[ \frac{f^2}{N^2(z)} \frac{dF_n}{dz} \right] &= -\lambda_n^2 F_n, \quad \text{with} \\ \frac{dF_n}{dz} \Big|_{z=0} &= \frac{dF_n}{dz} \Big|_{z=-H} = 0, \end{aligned} \quad (1)$$

where  $f$  is the Coriolis frequency,  $N(z)$  is the buoyancy frequency, and  $\lambda_n$  are the eigenvalues, fails in this respect. By construction, the functions  $F_n(z)$  are a complete basis in which to expand the streamfunction  $\psi$  of flows, provided they satisfy the same homogeneous boundary conditions, which imply zero surface and bottom buoyancy. But for realistic flows with nonzero surface buoyancy  $b = f\partial_z\psi|_{z=0}$ , expansion in baroclinic modes leads to a nonuniform convergence near  $z = 0$ , and a very large set of modes is required to capture the near-surface behavior.

As noted by Lapeyre and Klein (2006), in quasigeostrophic theory, the dynamical contribution of the surface buoyancy can be separated from that of the interior potential vorticity: taking advantage of the linearity of the inversion of the quasigeostrophic potential vorticity (PV)

$$q = \nabla^2\psi + \partial_z \left( \frac{f^2}{N^2} \partial_z\psi \right) \quad (2)$$

the streamfunction may be decomposed into interior and surface parts,  $\psi = \psi^{\text{int}} + \psi^{\text{surf}}$  (assuming zero buoyancy at the bottom), where  $\psi^{\text{int}}$  satisfies (2) with boundary

condition  $\partial_z\psi^{\text{int}}|_{z=0} = 0$  while  $\psi^{\text{surf}}$  satisfies the zero-PV condition  $\nabla^2\psi^{\text{surf}} + \partial_z(f^2/N^2\partial_z\psi^{\text{surf}}) = 0$  with  $\partial_z\psi^{\text{surf}}|_{z=0} = b/f$ . The vertical structure of the interior contribution can be expanded in the standard baroclinic modes. By contrast, the surface contribution—the only one retained in SQG theory—has a vertical structure determined by the zero PV condition, which couples horizontal and vertical dependence, reducing to  $\exp(\kappa Nz/f)$ , in the case of  $N$  constant and bottom depth  $H \gg f/(\kappa N)$ , where  $\kappa$  is the horizontal wavenumber modulus.

It is intuitively clear that an effective projection basis should somehow combine modes similar to the baroclinic modes with modes that, like the exponential modes of SQG theory, capture the dynamical contribution of the surface buoyancy. A systematic method to obtain such a basis has remained elusive, however. Tulloch and Smith (2009) proposed a heuristic model based on a barotropic and first baroclinic mode, appended by exponential modes for each surface. Similarly, Lapeyre (2009) attempted to represent the full dynamics of the upper ocean with a truncated set of standard baroclinic modes appended by an exponential surface mode. However, these hybrid modes do not diagonalize the energy, since the surface and interior modes are not orthogonal. Moreover, because the surface modes depend on wavenumber while the interior modes do not, the energetic overlap increases with increasing horizontal scale. These difficulties stem from the fact that the addition of the exponential mode makes the set of functions linearly dependent, thus the appended set of modes fails to be a basis. A consequence is that the modal decomposition is nonunique. Lapeyre (2009) defined a decomposition by requiring that it minimizes a certain functional, but the results remained inconclusive. An alternative basis, involving modes satisfying the Dirichlet condition  $\psi|_{z=0} = 0$  together with the barotropic mode, has recently been proposed by Scott and Furnival (2012), but this approach also suffers from a lack of orthogonality.

In this paper we derive a new family of bases that diagonalize the energy and effectively capture surface-intensified motion driven by buoyancy. There are infinitely many possible complete projection bases that diagonalize the energy, thus an additional constraint is needed to both retain this property and build in the efficient representation of surface dynamics. Our approach is to demand that the basis simultaneously diagonalizes both the energy and another quadratic invariant, a generalized potential enstrophy that includes the variances of the surface and bottom buoyancy fields. The relative weight of the potential enstrophy and upper and lower buoyancy variances in this invariant provide two new nondimensional parameters that determine the basis uniquely.

The interior problem that arises is similar to the standard vertical mode problem, but retains a dependence on horizontal wavenumber, and the eigenvalue appears in both the eigenvalue equation and its boundary conditions. In a limiting case, the standard baroclinic modes are recovered: for constant  $N$  and  $-H \leq z \leq 0$ , these are  $\psi_n \propto \cos(n\pi z/H)$ ,  $n = 0, 1, \dots$ . Another limiting case, motivated by the ocean where shears are concentrated near the upper surface but are weak at depth, leads to the simple basis

$$\psi_0 \propto \cosh\left[\frac{N\kappa(z+H)}{f}\right] \quad \text{and} \quad \psi_n \propto \sin\left[\frac{(2n-1)\pi z}{2H}\right]$$

for  $n = 1, 2, \dots$ , (3)

which includes the exponential mode of SQG theory.

The paper is organized as follows. In section 2 we describe the construction of a generalized eigenvalue problem that defines the new basis. In section 3, we derive analytical solutions and general results for two special cases: constant  $N$ , for expository purposes, and an ocean-like case, in which the lower boundary is assumed quiescent, leading to (3). Various bases are tested in section 4 on fields generated from a set of high-resolution quasigeostrophic simulations of baroclinic turbulence. Finally, we discuss and conclude in section 5. Mathematical details of the generalized eigenvalue problem are relegated to appendix A; the derivation of a discrete version of the modes is included in appendix B.

## 2. Surface-aware basis

Throughout the paper, we assume a horizontally periodic domain bounded vertically by rigid surfaces at  $z = z^-$  and  $z = z^+$ , with total depth  $H = z^+ - z^-$ . The assumption of horizontal periodicity allows us to Fourier transform the equations in the horizontal plane, resulting in separable dynamics and ordinary differential equations for the vertical structure. (In more general domains, the Fourier series can be replaced by an expansion in eigenfunctions of the horizontal Laplacian, and the results obtained here should hold essentially unchanged.) The complex amplitudes of the quasigeostrophic potential vorticity (PV)  $q = q_{kl}(z)$ , surface buoyancies (SBs)  $b_{kl}^\pm$ , and streamfunction  $\psi = \psi_{kl}(z)$  are then related by

$$\left(\frac{f^2}{N^2}\psi'\right)' - \kappa^2\psi = q, \quad z^- < z < z^+, \quad \text{and} \quad (4a)$$

$$\frac{f^2}{N^2H}\psi' = b^\pm, \quad z = z^\pm, \quad (4b)$$

where  $\kappa = (k^2 + l^2)^{1/2}$  is the wavenumber magnitude, a prime indicates a  $z$ -derivative,  $f$  is the Coriolis frequency, and  $N = N(z)$  is the buoyancy frequency. We include the nonstandard factor  $f^2/(N^2H)$  in (4b) so that the SBs and PV have the same dimension (inverse time), and because it ultimately yields a more natural eigenvalue problem. We have omitted the wavenumber subscript on  $q$ ,  $b^\pm$ , and  $\psi$  and continue to do so here onward.

The quasigeostrophic equation set has four quadratic invariants: energy, potential enstrophy, and the buoyancy variance at each surface. At each wavenumber  $\kappa$ , these are

$$E_\kappa = \frac{1}{2H} \int_{z^-}^{z^+} \left( \frac{f^2}{N^2} |\psi'|^2 + \kappa^2 |\psi|^2 \right) dz, \quad (5)$$

$$Z_\kappa = \frac{1}{2H} \int_{z^-}^{z^+} |q|^2 dz, \quad \text{and} \quad (6)$$

$$B_\kappa^\pm = \frac{1}{2} |b^\pm|^2. \quad (7)$$

Summing each quantity over  $(k, l)$  gives the total invariant.

We seek to define a complete basis that diagonalizes the energy. This can be done in infinitely many ways. Our strategy is based on the following principles: (i) we regard the energy as a functional, not of the streamfunction, but of the PV and of the SBs; and (ii) we exploit standard results on the simultaneous diagonalization of quadratic forms. Principle (i) is grounded in the quasigeostrophic model, which makes it explicit that PV and SBs, taken together, make up the set of dynamical variables. Thus, the contribution of the SBs to the dynamics is recognized; as a result, the bases we obtain naturally represent data with nonzero surface buoyancies. Regarding (ii), we recall a classical result from linear algebra: whereas there are infinitely many bases diagonalizing a quadratic form  $\mathbf{x}^T \mathbf{A} \mathbf{x}$ , where  $\mathbf{A}$  is a symmetric positive definite matrix, only one of these bases also diagonalizes another quadratic form  $\mathbf{x}^T \mathbf{B} \mathbf{x}$  (e.g., Horn and Johnson 1990). This is simply found by solving the generalized eigenvalue problem  $\mathbf{B} \mathbf{x} = \lambda \mathbf{A} \mathbf{x}$ . An analogous result applies to linear operators (see, e.g., Goldstein 1980). Similarly, here we can define a unique basis by insisting that it diagonalizes another quadratic form in addition to the energy  $E_\kappa$ . A natural choice for this is a ‘‘generalized potential enstrophy’’ that combines the remaining invariants into a single quantity,

$$P_\kappa \equiv Z_\kappa + \alpha_+ B^+ + \alpha_- B^-, \quad (8)$$

where  $\alpha_\pm > 0$  are (nondimensional) undetermined weights, the choice of which will be discussed later. This approach yields a unique basis for fixed  $\alpha_\pm$ .

To proceed, we require four objects: a vector structure that combines the SBs and interior PV, an inner product that operates on this vector, and two operators (analogous to the matrices **A** and **B** above) that give the energy and generalized potential enstrophy in terms of the inner product. The construction of these objects, and the derivation of the generalized eigenvalue problem that simultaneously diagonalizes  $E_\kappa$  and  $P_\kappa$ , is relegated to appendix A. The outcome is the eigenvalue problem

$$\left(\frac{f^2}{N^2}\phi_n'\right)' - \kappa^2\phi_n = -\mu_n^2\phi_n$$

$$\text{with } \frac{f^2}{N^2H}\phi_n' = \pm \frac{\mu_n^2}{\alpha_\pm}\phi_n \text{ at } z = z^\pm, \quad (9)$$

where the eigenvalues  $\mu_n$  and eigenfunctions  $\phi_n(z)$  are purely real. The eigenfunctions describe the vertical structure of the streamfunction of each mode; they are orthonormal in the sense that (cf. 5)

$$\frac{1}{H} \int_{z_-}^{z_+} \left(\frac{f^2}{N^2}\phi_m'\phi_n' + \kappa^2\phi_m\phi_n\right) dz = \delta_{mn}. \quad (10)$$

The choice of normalization, and two additional orthogonality conditions, is discussed in appendix A; the above relation has the advantage that the weights  $\alpha_\pm$  do not appear.

The eigenvalue problem (9) is a key result of the paper, and its eigenfunctions  $\phi_n(z)$  can be used as a projection basis. Given a streamfunction  $\psi$ , one can write

$$\psi = \sum_n a_n \phi_n, \quad (11)$$

where  $a_n$  are amplitude coefficients. Using the orthogonality relation (10), the amplitudes are given by

$$a_n = \frac{1}{H} \int_{z_-}^{z_+} \left(\frac{f^2}{N^2}\phi_n'\psi' + \kappa^2\phi_n\psi\right) dz \quad (12)$$

(alternate forms of  $a_n$  are also possible, using the other orthogonality conditions presented in appendix A). The energy and generalized potential enstrophy are then

$$E_\kappa = \frac{1}{2} \sum_n |a_n|^2 \quad \text{and} \quad P_\kappa = \frac{1}{2} \sum_n \mu_n^2 |a_n|^2, \quad (13)$$

respectively.

Note that, even though the eigenvalue problem (9) is not of the standard Sturm–Liouville form, because of the presence of the eigenvalue  $\mu_n^2$  in the boundary conditions (a condition that also arises in the free-boundary baroclinic instability problem considered by Ripa 2001), the basis of eigenvectors can be shown to be complete; this is discussed further in appendix A.

Lastly, note that our choice of orthogonality conditions implies slightly unfamiliar dimensions for the eigenfunctions. Because  $[q], [b^\pm] \sim [T^{-1}]$  and  $[\mu] \sim [L^{-1}]$  (where  $T$  is time,  $L$  is length, and braces mean ‘‘dimensions of’’), the orthogonality condition (10) demands  $[\phi] \sim [L]$ .<sup>1</sup> In the next section, the problem will be analyzed in an appropriate nondimensional form.

### 3. Structure of the surface-aware modes and special cases

The approach described above provides a family of bases parameterized by the values of  $\alpha_+$  and  $\alpha_-$ . In principle, different values can be chosen for different wavenumbers  $\kappa$ ; here, however, we restrict attention to choices of  $\alpha_\pm$  that are independent of  $\kappa$ . To clarify some general properties of the new modes, we first recast the eigenvalue problem in nondimensional form with the substitutions  $z \mapsto Hz, \kappa \mapsto f/(N_0H)\kappa$  and  $\mu \mapsto f/(N_0H)\mu$ , where  $N_0$  is a typical value of  $N$ ; thus the wavenumber and eigenvalue are scaled by the approximate deformation length,  $N_0H/f$ . The nondimensional eigenvalue problem (9) then becomes

$$(s\phi_n')' = -\lambda_n^2\phi_n$$

$$\text{with } s\phi_n' = \pm \frac{\lambda_n^2 + \kappa^2}{\alpha_\pm}\phi_n \text{ at } z = 0, -1,$$

$$\text{where } s = \frac{N_0^2}{N^2(z)} \quad (14)$$

and we have defined an alternative eigenvalue  $\lambda_n$  such that

$$\mu_n^2 = \kappa^2 + \lambda_n^2. \quad (15)$$

Written in terms of  $\lambda_n$ , the eigenvalue equation takes the form of the standard vertical mode equation, but with more complicated boundary conditions.

Analysis of the new eigenvalue problem (14) is complicated by its dependence on three independent parameters:  $\kappa, \alpha_+$ , and  $\alpha_-$ . For each choice of parameters, there is an infinite set of eigenvalues. Since the problem depends on the two weights  $\alpha_\pm$  in a nearly equivalent way, we proceed first by setting the weights equal and defining  $\alpha \equiv \alpha_+ = \alpha_-$  (a case in which the weights differ

<sup>1</sup> One indirect consequence of this choice is that the expansion coefficients  $a_n$  are identical for both the streamfunction  $\psi(z)$  and the potential vorticity  $q(z)$ . This is in contrast to the typical method of expansion in the standard vertical modes  $F_n(z)$  from (1): if  $\psi(z) = \sum_n \Psi_n F_n(z)$  and  $q(z) = \sum_n Q_n F_n(z)$ , then  $Q_n = -(\kappa^2 + \lambda_n^2)\Psi_n$  (e.g., Hua and Haidvogel 1986).

will be considered in a later subsection). The nature of the eigenproblem is then largely determined by the size of the boundary condition coefficient  $\mu_n^2/\alpha$ : when  $\mu_n^2/\alpha \rightarrow 0$ , the boundary conditions revert to the standard case  $\phi'_n = 0$  at the top and bottom, while when  $\mu_n^2/\alpha \rightarrow \infty$ , the boundary conditions become  $\phi_n = 0$  at the top and bottom. However, more subtle possibilities arise as well because, unlike in the standard vertical mode problem,  $\lambda_n$  may be imaginary (although  $\mu_n$  is always real). When  $\lambda_n$  is real, the modes are oscillatory, but when it is imaginary, the modes are evanescent—these can be interpreted either as surface modes or as extensions of the barotropic mode.

This interpretation is suggested by examining the eigenvalue problem in two limiting regimes:

$\kappa^2 \ll \alpha$ : modes with real  $\lambda$  satisfy the simplified boundary condition  $(s\phi'_n) = \pm \lambda_n^2 \phi_n / \alpha$  at  $z = 0, -1$  which further reduces to  $\phi'_n = 0$  for  $\alpha \gg 1$ , corresponding to the standard baroclinic modes.<sup>2</sup> These are complemented by a barotropic mode for which the first approximation  $\lambda = 0$  can be refined to the purely imaginary  $\lambda = i\kappa\sqrt{2/\alpha}$ .

$\kappa^2 \gg \alpha$ : In this case, almost all modes have  $\mu_n^2 = \kappa^2 + \lambda_n^2 \gg \alpha$  and hence satisfy the simplified boundary conditions  $\phi_n = 0$  at  $z = 0, -1$ . There are two additional modes, however, for which  $\mu_n^2 = O(\alpha)$  and hence  $\lambda \sim i\kappa$ . These solve

$$(s\phi'_n)' - \kappa^2 \phi_n \simeq 0$$

$$\text{with } s\phi'_n = \pm \frac{\mu_n^2}{\alpha_{\pm}} \phi_n \text{ at } z = 0, -1, \quad (16)$$

and can be recognized as surface modes, with zero interior PV.

*a. Analytical solutions for constant N*

In the special case of constant stratification, or  $s = 1$ , the eigenvalue problem (14) can be solved in closed form. Writing the solutions as

$$\phi_n = A \cos(\lambda_n z) + B \sin(\lambda_n z),$$

where  $A$  and  $B$  are integration constants, and imposing the boundary conditions leads to an algebraic equation for  $\lambda_n$ , which may be either real or imaginary. For  $\lambda_n^2 > 0$ , the characteristic equation (dropping the subscript  $n$ ) is

<sup>2</sup> This approximation is not uniform in  $n$  but breaks down for highly oscillatory modes, with  $\lambda_n = O(\alpha)$ , which satisfy  $\phi' = O(\alpha) \neq 0$  at  $z = 0, -1$  and thus differ from the standard high- $n$  baroclinic modes.

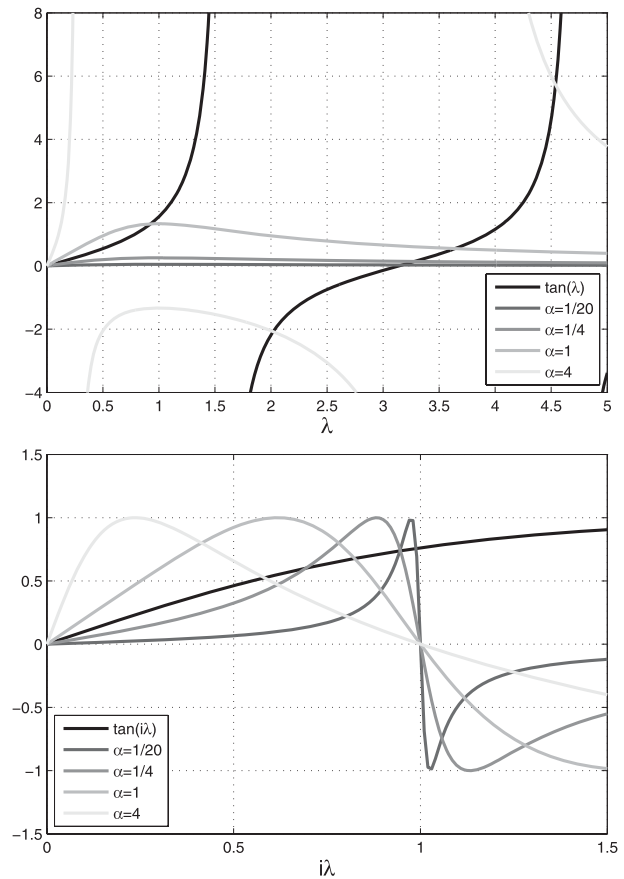


FIG. 1. Graphical solutions for eigenvalues with constant  $N$  for  $\kappa = 1$ . (left) The left- and right-hand sides of Eq. (17) and (right) Eq. (18) are shown.

$$\tan \lambda = \frac{(\alpha_+ + \alpha_-)\lambda(\lambda^2 + \kappa^2)}{(\lambda^2 + \kappa^2)^2 - \alpha_+ \alpha_- \lambda^2}. \quad (17)$$

For  $\lambda^2 < 0$  we define  $\tilde{\lambda} = i\lambda$  and obtain

$$\tanh \tilde{\lambda} = \frac{(\alpha_+ + \alpha_-)\tilde{\lambda}(\kappa^2 - \tilde{\lambda}^2)}{(\kappa^2 - \tilde{\lambda}^2)^2 + \alpha_+ \alpha_- \tilde{\lambda}^2}. \quad (18)$$

Equations (17) and (18) are suitable for a graphical analysis. Figure 1 shows that there are infinitely many solutions to (17) (top panel) and one or two solutions to (18) depending on  $\alpha_{\pm}$  (bottom panel; in both cases we set  $\alpha \equiv \alpha_+ = \alpha_-$ ). An important parameter is the ratio of the slopes of the right- and left-hand sides of (17) and (18) at  $\lambda = 0$ , which in both cases is

$$\frac{\alpha_+ + \alpha_-}{\kappa^2} \equiv \tilde{\kappa}^{-2}.$$

When  $\tilde{\kappa} < 1$  there is only one solution to (18), and there is a solution of (17) with  $\lambda < \pi/2$ . On the other hand, if

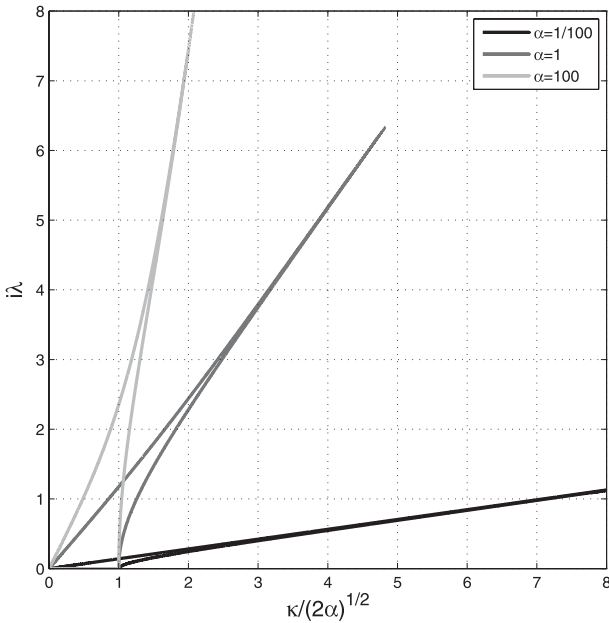


FIG. 2. Solutions to (18), with  $\kappa$  scaled by  $\sqrt{2\alpha}$ , the cutoff separating cases with one or two solutions for imaginary  $\lambda$ .

$\tilde{\kappa} > 1$ , there are two solutions to (18) (note that the maximum of the right-hand side of (18) is 1), and there may or may not be a solution of (17) for  $\lambda < \pi/2$ .<sup>3</sup>

The solution to (18) gives either a generalization of the barotropic mode, in the case of a single solution, or two modes that capture the vertical structure of the surface modes. Setting  $\alpha \equiv \alpha_+ = \alpha_-$ , these solutions are plotted as functions of  $\tilde{\kappa}$  in Fig. 2: there are two solutions when  $\tilde{\kappa} > 1$ , but only one otherwise. The limiting solutions discussed in the previous section can be derived explicitly. In the limit  $\tilde{\kappa}^2 = \kappa^2/(2\alpha) \ll 1$ , the single solution of (18) is given by  $\tilde{\lambda} \sim \kappa\sqrt{2/\alpha}$ , with eigenfunction  $\phi \propto 1$ , which can be interpreted as the barotropic mode. For  $\tilde{\kappa}^2 \gg 1$ , the two solutions can be identified as surface intensified modes, one symmetric and the other antisymmetric about the center of the domain, explicitly given by

$$\phi_0 \propto \cosh\left[\kappa\left(z + \frac{1}{2}\right)\right] \quad \text{and} \quad \phi_1 \propto \sinh\left[\kappa\left(z + \frac{1}{2}\right)\right],$$

with eigenvalues  $\mu_0/\alpha = \kappa \tanh\kappa$  and  $\mu_1/\alpha = \kappa \coth\kappa$ . For  $\kappa \gg 1$ , the eigenvalues are nearly identical, so that linear combinations of the eigenfunctions will also satisfy the

<sup>3</sup> Note also that, if  $\alpha_+\alpha_- > 4\kappa^2$ , the denominator of the right-hand side of (17) goes to 0, but stays finite otherwise: the existence of a 0 in the denominator determines whether there is a solution to (17) with  $\lambda < \pi/2$  in the case  $\tilde{\kappa}^{-2} > 1$ .

eigenvalue problem—in particular, one can construct separate upper-surface and lower-surface modes. For real  $\lambda$ , the right-hand side of (17) tends to zero for both large and small  $\kappa$ , leading to eigenvalues  $\lambda_n = n\pi$ ,  $n = 1, 2, \dots$ . The eigenfunctions, however, differ in the two cases: for  $\tilde{\kappa} \ll 1$ , they have the standard form  $\phi_n \propto \cos(n\pi z)$ , but for  $\tilde{\kappa} \gg 1$ , they are  $\phi_n \propto \sin(n\pi z)$ . The first four modes, for  $\alpha = 1$  and a range of  $\kappa$  are plotted in Fig. 3.

*b. An oceanic special case*

Here we consider a case that is potentially the most relevant to the ocean, where shears near the surface may lead to surface-intensified modes, while the quiescent abyss may be more naturally represented by the standard boundary condition,  $\phi' = 0$  at the bottom. The relevant limits for this case are  $\alpha_+ \ll 1$  and  $\alpha_- \rightarrow \infty$ , in which case the eigenvalue problem reduces to

$$(s\phi'_n)' = -\lambda_n^2\phi_n, \quad \text{with} \quad \phi_n|_{z=0} = 0, \quad \phi'_n|_{z=-1} = 0, \tag{19a}$$

and

$$(s\phi'_0)' - \kappa^2\phi_0 = 0, \\ \text{with} \quad s\phi'_0|_{z=0} = \frac{\mu_0^2}{\alpha_+}\phi_0, \quad \phi'_0|_{z=-1} = 0. \tag{19b}$$

to leading order in  $\alpha_+$ . The solutions  $\phi_n$ ,  $n = 1, 2, \dots$  to (19a) describe interior modes, while  $\phi_0$  is the solution to (19b) with  $\mu_0^2/\alpha_+ = O(1)$  and represents a zero PV, surface-intensified mode.

Note that the structure of the interior modes, like that of the standard baroclinic modes, is independent of  $\kappa$ ; the normalization of the mode energy that we have chosen however leads to  $\kappa$ -dependent normalization factors. Since we concentrate on the leading-order approximation to the eigenvalue problem as  $\alpha_+ \rightarrow 0$ , all the modes, including the surface-intensified one, are independent of  $\alpha_+$  and so are the normalization factors (because the energy does not involve  $\alpha_+$ ). Only the eigenvalue  $\mu_0^2$  depends (linearly) on  $\alpha_+$ , although the approximation  $\mu_0^2 = 0$  can be made to conclude, in particular, that the surface-intensified mode has a generalized enstrophy which vanishes to leading order.

Recently, Scott and Furnival (2012) proposed to use the eigenfunctions of (19a), forming what they term a Dirichet basis, in conjunction with the barotropic mode. While this set of functions, like that obtained by adding a surface mode to the standard baroclinic basis (Lapeyre 2009), does not diagonalize the energy, it is remarkable that this is achieved by the complete set of solutions of (19a) and (19b), that is, by the Dirichlet basis plus a surface mode.

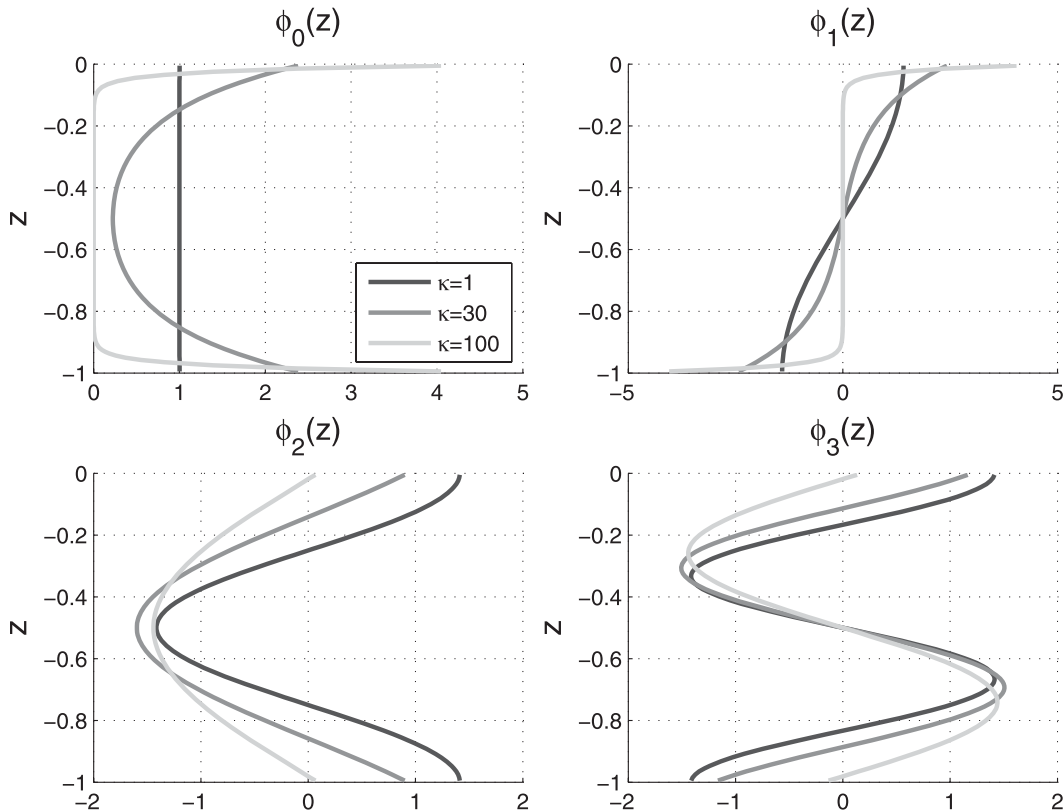


FIG. 3. The first four eigenfunctions  $\phi_n$  for the constant- $N$  case, with  $\alpha_+ = \alpha_- = 100$  and  $\kappa = 1, 30, 100$ .

For constant  $N$  (or  $s = 1$ ), the solutions to (19) may be computed explicitly; they are

$$\phi_0 = A \cosh[\kappa(z + 1)], \quad A \equiv \sqrt{\frac{2}{\kappa \sinh(2\kappa)}}, \quad \text{and} \quad (20a)$$

$$\phi_n = B \sin\left[\left(n - \frac{1}{2}\right)\pi z\right], \quad B \equiv \sqrt{\frac{2}{\pi^2(n - 1/2)^2 + \kappa^2}}, \quad (20b)$$

with eigenvalues  $\mu_0^2 = \alpha_+ \kappa \tanh \kappa$  (corresponding to  $\tilde{\lambda} \simeq \kappa - (\alpha_+/2) \tanh \kappa$ ) and  $\lambda_n = (n - 1/2)\pi$  with  $n = 1, 2, \dots$ . Their dimensional form is given by (3) in the introduction. Again, note that the dependence on  $\kappa$  of the coefficient for the interior modes is due to the normalization choice but is irrelevant for the projection of data.

#### 4. Application to the projection of simulated data

As a demonstration, we use the new basis to project the energy in three simulated turbulent flows, each generated by baroclinic instability of a fixed mean state in a horizontally periodic quasigeostrophic model. The numerical model is spectral in the horizontal, and

finite-difference in the vertical—it is the same as used in, for example, Smith and Ferrari (2009). Energy is dissipated by linear bottom drag, and enstrophy is removed by a highly scale-selective exponential cutoff filter (Smith et al. 2002). In all cases, the model resolution is  $512 \times 512 \times 100$ .

We analyze results from three simulations. These first two are based on highly idealized flows, and will be used to demonstrate the fundamental structure of the basis, and how the partition of energy depends on both the nature of the flow, and on the choice of the non-dimensional weights  $\alpha_{\pm}$ . The third simulation is based on a more realistic, ocean-like mean state, and is designed to explore the oceanic special case considered at the end of the last section. To project the simulated data onto the new basis, one must consider the generalized matrix eigenvalue problem that results from the particular vertical discretization used in the model. The details of the construction of the basis in this discretization are given explicitly in appendix B.

##### a. Idealized “interior” and “surface” baroclinic instability simulations

Both idealized flows have constant stratification  $s = 1$ , a ratio of domain scale to deformation scale equal to 4

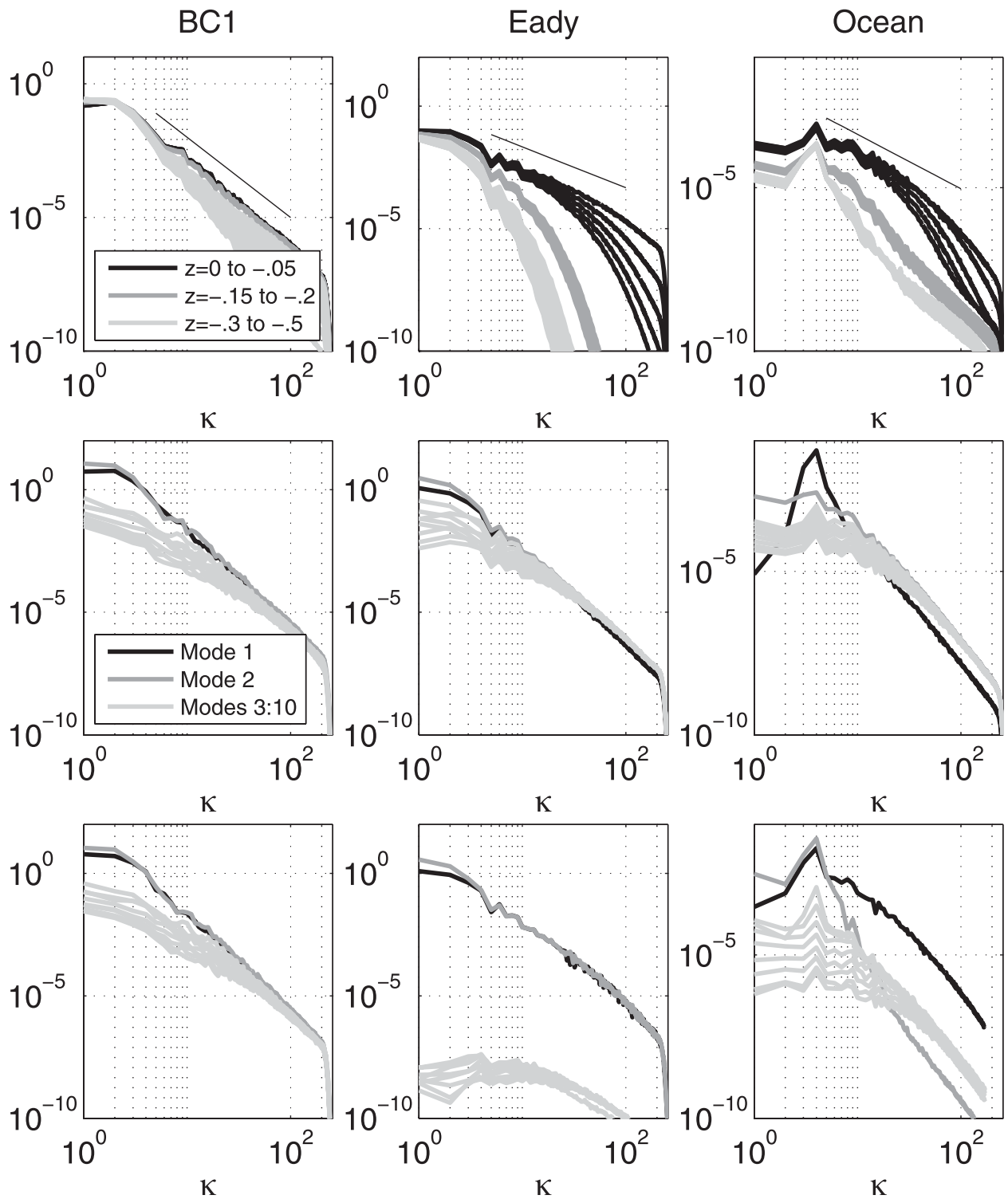


FIG. 4. Energy spectra for the (left) BC, (middle) Eady, and (right) Ocean simulations. (top) Spectra for selected vertical levels (see legend). (middle) Spectra from fields projected onto standard vertical modes (modes 1, 2 and 3–10 are shown). (bottom) Spectra from fields projected onto new modes, with  $\alpha_+ = \alpha_- = 10^6$  for the BC1 case,  $\alpha_+ = \alpha_- = 10^{-4}$  for the Eady case, and  $\alpha_+ = 2, \alpha_- = 10^6$  for the Ocean case.

and  $\beta = 0$ , but mean states that generate different types of baroclinic instability. The first simulation, is forced by an “interior instability,” with a mean flow that projects onto the first (standard) baroclinic mode,  $U(z) = \cos\pi z$ . Flows of this type are unstable owing to a sign change of the mean interior PV gradient, but have no mean SB gradients, since  $B_y^\pm \propto U_z|_{z=0,-1} = 0$ —we refer to this simulation as BC1. The second flow is forced by an Eady mean state, with a linear mean shear  $U(z) = z$ , so the instability is driven by mean SB gradients  $B_y^\pm = 1$ , resulting in energy generation near the two surfaces.

The simulations are run to statistically steady state, and snapshots of the steady-state prognostic fields of each are used to compute horizontal (total) energy spectra. The upper panels of Fig. 4 display the horizontal spectra for the BC1 (left) and Eady (middle) simulations for a few vertical levels  $z$  (the right-hand column plots will be discussed in the next subsection). It is immediately apparent that the energy in the BC1 simulation is spread rather evenly over depth; by contrast, the energy in the Eady simulation is largely concentrated at the two surfaces. The panels in the middle row of Fig. 4 show the first few modes of the energy projected onto the standard basis,  $\phi_n(z) \propto \cos(n\pi z)$ ,  $n = 1, 2, \dots$  (the baroclinic modes) and  $\phi_0 \propto 1$  (the barotropic mode). Consistent with the  $z$ -dependence of the energy in the upper panel, the energy in BC1 is largely captured by the barotropic and first baroclinic modes. By contrast, the energy in the Eady case seems to be distributed evenly across the barotropic and a large number of baroclinic modes, effectively demonstrating the failure of the standard modes to provide any insight into the energy partition in a case with large energy near the surfaces.

The bottom panels of Fig. 4 display the energy spectra for the first few modes in the projection onto the new basis (BC1, left panel; Eady, middle panel). Anticipating that the BC1 simulation is best represented by the standard baroclinic basis (recovered from the generalized basis in the limit  $\alpha_\pm \gg 1$ ), while the Eady simulation is best represented on the generalized basis in the limit  $\alpha_\pm \ll 1$ , we chose  $\alpha_\pm = 10^6$  for the former and  $\alpha_\pm = 10^{-4}$  for the latter. As is apparent, the generalized basis with the appropriate weights more efficiently captures the surface energy in the Eady simulation much better than the standard basis.

To quantify the choice of  $\alpha_\pm$ , we consider the projection of energy in both the BC1 and Eady simulations with the generalized basis using weights ranging from  $\alpha_\pm = 10^{-3}$  to  $10^3$  (always holding  $\alpha = \alpha_+ = \alpha_-$ ) and ask, for what weights is the energy captured by the least number of modes? A simple diagnostic for this, the ratio of the energy contained in the first two modes to the total energy as a function of  $\alpha$ , is shown in Fig. 5.

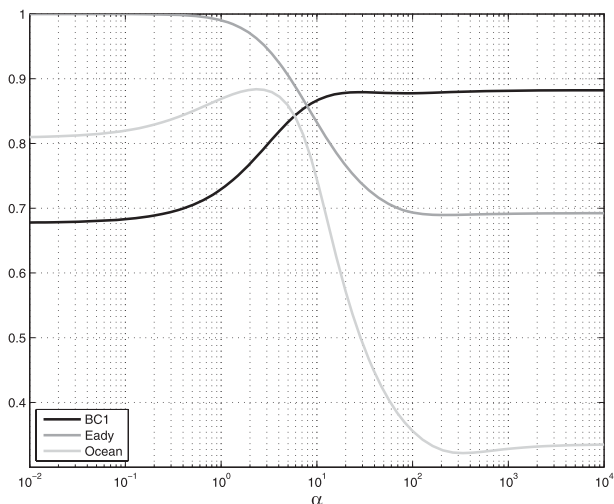


FIG. 5. Ratio of the energy content of the first two modes to the total energy as a function of  $\alpha = \alpha_+ = \alpha_-$  for the BC1 and Eady simulations, and as a function of  $\alpha = \alpha^+$  (with  $\alpha_- \rightarrow \infty$ ) for the Ocean simulation.

results indicate that extreme values of  $\alpha$  are best suited for the BC1 ( $\alpha \rightarrow \infty$ ) and Eady ( $\alpha \rightarrow 0$ ) simulations, thus confirming our choice for Fig. 4. In the next section we examine a third simulation where the interior and surface contributions are more balanced, so that intermediate values of  $\alpha_{\pm}$  may be expected to be relevant.

#### b. A semirealistic oceanic simulation

The third simulation is driven by a mean state typical of the midlatitude ocean. It uses an exponential mean stratification  $N^2 = N_0^2 \exp(z/h)$ , so that  $s = \exp(-z/h)$ , with  $h = 0.2$ , intended to represent the pycnocline. The mean shear is  $U(z) = h(z + 1 - h) \exp(z/h) + g(z) + C$ , where  $g(z)$  is the first standard baroclinic eigenfunction of the operator  $(sg')' = -\lambda^2 g$ , with  $g' = 0$  at  $z = 0, -1$ , so that  $U$  is surface-intensified with  $U'(0) = 1$  and  $U'(-1) = 0$ . The constant  $C$  is set to ensure  $\int_{-1}^0 U(z) dz = 0$ . Both  $U(z)$  and  $N(z)$  are plotted in the top panel of Fig. 6. Note that  $U$  is baroclinically unstable because of both an internal sign change of the mean PV gradient, and to the interaction of the mean interior PV gradient  $Q_y$  with the mean upper SB gradient  $B_y^+$ . Consistent with the assumptions of the ocean modes, the lower SB gradient  $B_y^- = 0$ . The ratio of the domain scale to the first baroclinic deformation radius (as determined by  $\lambda^{-1}$ ) is 5. The nondimensional Coriolis gradient  $\beta U_0 L_D^{-2} = 1.2$ , and energy is dissipated by a linear drag  $rL_d U_0^{-1} = 0.4$ . The steady-state turbulent flow has a complicated vertical structure, as evidenced by the vertical slice of the PV shown in Fig. 7.

The energy spectra for the flow are shown in the right panels of Fig. 4, just as for the BC1 and Eady cases. The

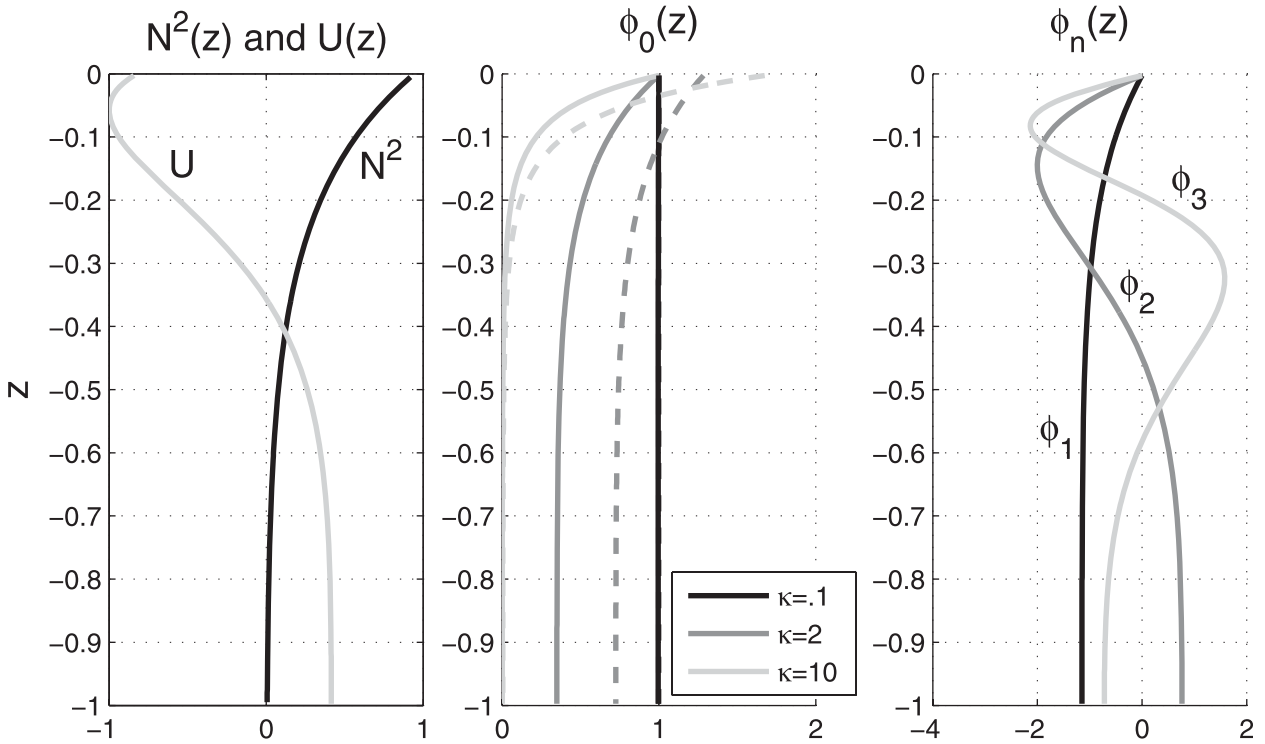


FIG. 6. (left)  $N^2(z)$  and  $U(z)$  for the Ocean simulation. (middle) The surface mode  $\phi_0(z)$  with  $\alpha_- \rightarrow \infty$  and  $\alpha_+ \ll 1$  (solid) and  $\alpha_+ = 2$  (dashed), for a range of wavenumbers  $\kappa$  (see legend). The  $\kappa = 0.1$  lines are on top of each other. (right) The first three interior modes with  $\alpha_+ \ll 1$  and  $\alpha_- \rightarrow \infty$ .

energy spectra by vertical level again indicates a very surface-intensified flow, but this time, the flow falls off from a  $-5/3$  spectral slope to a more energetic interior than was the case for the Eady simulation. Projection onto the standard vertical modes (middle right panel) indicates a peak in the barotropic mode, but otherwise energy is spread evenly over a large number of baroclinic modes. Projection onto a generalized basis is shown in the bottom right panel. For this simulation with no buoyancy activity at the bottom, it is natural to use a basis with  $\alpha_- \rightarrow \infty$ . The maximum in the ratio of the energy in modes 1 and 2 to total energy shown in Fig. 5

suggests that the value  $\alpha = \alpha_+ = 2$  is appropriate. The first few modes of the corresponding basis are shown in the bottom panels of Fig. 6. This is the basis chosen for Fig. 4, and indicates that the projection is very effective, with most of the energy captured by the surface and modified first baroclinic modes. An alternative basis is the ‘oceanic’ basis of section b which takes  $\alpha_+ \ll 1$ . The spectra obtained with this basis (not shown) are essentially identical to those obtained for  $\alpha_+ = 2$ . This suggests that the results are insensitive to the precise value of  $\alpha_+$  and that ‘oceanic’ basis may be a good default choice to analyze typical ocean data.

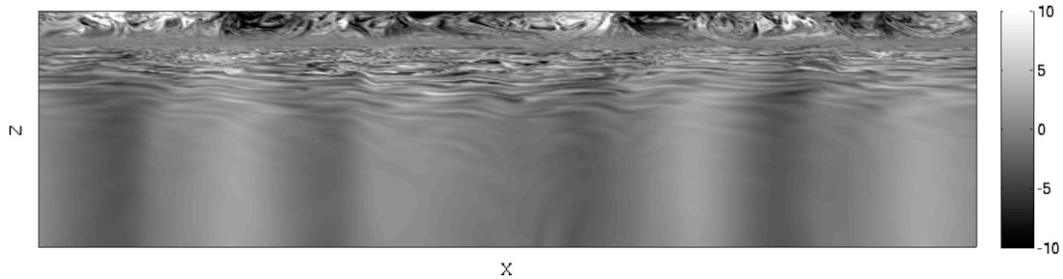


FIG. 7. Vertical slice of PV snapshot from the Ocean simulation. The flow has a complicated structure in the upper ocean, masking a more uniform flow at depth.

## 5. Conclusions

This paper presents a family of basis functions designed for the projection of three-dimensional ocean velocity data. The bases diagonalize both the quasigeostrophic energy and a generalization of the quasigeostrophic potential enstrophy that includes contributions from the buoyancy variances at the upper and lower surfaces. The family of bases is parameterized by the weights  $\alpha_{\pm}$  assigned to the surface buoyancy variances—the standard baroclinic modes are recovered in the limit  $\alpha_{\pm} \rightarrow \infty$ , but the modes obtained in the opposite limit allow for efficient representation of the surface buoyancy variances. The bases should prove advantageous in a number of applications, from projection of observations to the derivation of highly truncated theoretical models. Their main drawback compared to the standard basis of baroclinic modes is the dependence of the modes on the wavenumber  $\kappa$ , which implies a lack of separation between the horizontal vertical structure in physical space. This drawback is unavoidable if some of the modes are to reflect the SQG contribution; it is minimized for the “oceanic” basis obtained for  $\alpha_{+} \rightarrow 0$ ,  $\alpha_{-} \rightarrow \infty$  since all but one modes have a  $\kappa$ -independent structure.

The limit  $\alpha_{-} \rightarrow \infty$  would seem a natural choice of generalized basis for typical ocean conditions takes because of the relative lack of buoyancy activity at the bottom. Regarding  $\alpha_{+}$ , an optimal value can in principle be chosen by inspecting the spectra for a range of values or by using a diagnostic such as that of Fig. 5. However, some simpler rules of thumb would be desirable. Intuitively, one might expect that the optimal values of  $\alpha_{\pm}$  are those that balance the contributions of the enstrophy  $Z_{\kappa}$  and of the surface-buoyancy variance  $B_{\kappa}^{+}$  in the generalized enstrophy  $P_{\kappa} = Z_{\kappa} + \alpha_{+}B_{\kappa}^{+}$ . Some support for this intuition is provided by Fig. 8 which shows  $Z_{\kappa}$ ,  $B_{\kappa}^{+}$  and their ratio as a function of  $\kappa$  for the ocean simulation. The figure shows a ratio  $Z_{\kappa}/B_{\kappa}^{+}$  that is around 5 for a broad range of  $\kappa$ , roughly consistent with the value  $\alpha_{+} = 2$  indicated by Fig. 5. There is, however, a peak around  $\kappa = 4$  and a substantial increase for  $\kappa \gtrsim 20$ , which suggest that better results could be obtained by allowing  $\alpha_{+}$  to depend on  $\kappa$ . We have not explored this intriguing possibility here.

As an alternative to the ratio  $Z_{\kappa}/B_{\kappa}^{\pm}$ , it would be useful to relate more directly the value of the weights  $\alpha_{\pm}$  most appropriate to project a flow on the large-scale characteristics of the flow. Since for flows driven by instabilities,  $Z_{\kappa}$  and  $B_{\kappa}^{\pm}$  are related to the large-scale PV and surface-buoyancy gradients  $Q_y$  and  $B_y^{\pm}$ , it is plausible that the ratio  $Q_y/B_y^{\pm}$  can be used as a guide for the choice of the weights.

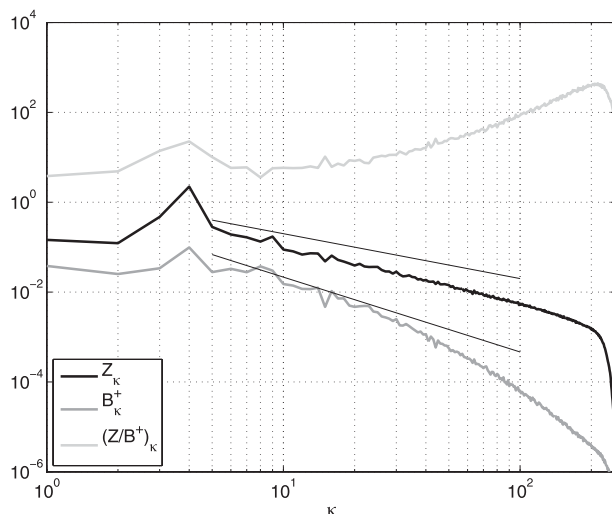


FIG. 8. Enstrophy  $Z_{\kappa}$  and surface buoyancy variance  $B_{\kappa}^{+}$  as functions of wavenumber  $\kappa$  for the Ocean simulation (lines with slopes  $-1$  and  $-5/3$  are included for reference). The ratio  $Z_{\kappa}/B_{\kappa}^{+}$ , also shown, can be used to guide the choice of the weight  $\alpha_{+}$  for an effective projection basis.

The advent of higher-resolution satellite observations, expected when the Surface Water Ocean Topography satellite becomes operational (Fu and Ferrari 2008), will improve our understanding of upper-ocean submesoscale dynamics only to the extent that we can connect surface observations with the three-dimensional structure of the flow below the surface. The basis derived and demonstrated here may prove a useful tool in this goal.

*Acknowledgments.* KSS acknowledges the support of both NSF Award OCE-0962054 and ONR Award N00014-09-01-0633, and helpful conversations with Ian Grooms, Shane Keating, and Xiao Xiao. JV acknowledges the support of a Leverhulme Research Fellowship, the hospitality of the Courant Institute, where this research was initiated, and Grant NE/J022012/1 of the U.K. Natural Environment Research Council.

## APPENDIX A

### Derivation and Properties of the Modes

#### a. Definitions

To construct the generalized eigenvalue problem, we define a vector, an inner product, and two operators, as follows.

#### 1) GENERALIZED POTENTIAL VORTICITY VECTOR

$$\mathbf{Q} \equiv \begin{bmatrix} b^{+} \\ q(z) \\ b^{-} \end{bmatrix}. \quad (\text{A1})$$

2) INNER PRODUCT

$$\langle \mathbf{Q}_1, \mathbf{Q}_2 \rangle = \frac{1}{H} \int_{z^-}^{z^+} \bar{q}_1 q_2 dz + \bar{b}_1^+ b_2^+ + \bar{b}_1^- b_2^-, \quad (\text{A2})$$

where an overbar denotes a complex conjugate. The specific choice of inner product is unimportant for the final results; this seemed the simplest choice.

3) ENERGY AND GENERALIZED POTENTIAL ENSTROPY OPERATORS

$$\mathcal{E}\mathbf{Q} = \begin{bmatrix} \psi(z^+) \\ -\psi(z) \\ -\psi(z^-) \end{bmatrix} \quad \text{and} \quad \mathcal{P}\mathbf{Q} = \begin{bmatrix} \alpha_+ b^+ \\ q(z) \\ \alpha_- b^- \end{bmatrix}, \quad (\text{A3})$$

where the streamfunction  $\psi$  is the solution of (4), given  $q$  and  $b^\pm$ , and the operators  $\mathcal{E}$  and  $\mathcal{P}$  are positive definite and self-adjoint (see below).

With the four definitions above, the energy and generalized potential enstrophy are

$$E_\kappa = \frac{1}{2} \langle \mathbf{Q}, \mathcal{E}\mathbf{Q} \rangle \quad \text{and} \quad P_\kappa = \frac{1}{2} \langle \mathbf{Q}, \mathcal{P}\mathbf{Q} \rangle, \quad (\text{A4})$$

respectively. The first of these expressions is obtained after an integration by parts, while the second is immediate.

Notice that our vector  $\mathbf{Q}$  bears a resemblance to the generalized potential vorticity of Bretherton (1966),

$$Q_B = \left( \frac{f^2}{N^2} \psi' \right)' - \kappa^2 \psi - \frac{f^2}{N^2} \psi' \delta(z - z^+) + \frac{f^2}{N^2} \psi' \delta(z - z^-).$$

The formalism presented in this paper treats the PV and SBs as independent functions, however.

*The generalized eigenvalue problem*

The basis we seek is now given by the eigenfunctions  $\xi_n$  of the generalized eigenvalue problem

$$\mathcal{P}\xi_n = \mu_n^2 \mathcal{E}\xi_n, \quad (\text{A5})$$

where the eigenvalues  $\mu_n^2$  are positive for all  $n$ . To obtain an explicit form for (A5), we define the components of  $\xi_n = [\xi_n^+, \xi_n(z), \xi_n^-]^T$  analogous to those of  $\mathbf{Q}$ , and scalar functions  $\phi_n(z)$  analogous to the streamfunction  $\psi$ , such that  $\mathcal{E}\xi_n = [\phi_n(z^+), -\phi_n(z), -\phi_n(z^-)]^T$ . In terms of these, the eigenvalue problem reads

$$\begin{bmatrix} \alpha_+ \xi_n^+ \\ \xi_n(z) \\ \alpha_- \xi_n^- \end{bmatrix} = \mu_n^2 \begin{bmatrix} \phi_n(z^+) \\ -\phi_n(z) \\ -\phi_n(z^-) \end{bmatrix}. \quad (\text{A6})$$

Using (4) to substitute  $\phi_n$  for the components of  $\xi_n$ , the problem can be written as in (9), whose eigenfunctions  $\phi_n$  are purely real. The three components of  $\xi_n$  may be derived from  $\phi_n$  using (A6), although in practice this is not necessary; data can be projected using the scalar eigenfunctions  $\phi_n$ .

*b. Orthogonality relations*

By construction, the eigenfunctions are orthogonal for the products  $\langle \cdot, \mathcal{E} \cdot \rangle$  and  $\langle \cdot, \mathcal{P} \cdot \rangle$ . The choice of normalization for the eigenvectors  $\xi_n$  is inconsequential, but it is convenient to fix the energy of each mode to be unity, that is, to take

$$\langle \xi_m, \mathcal{E}\xi_n \rangle = \frac{1}{H} \int_{z^-}^{z^+} \left( \frac{f^2}{N^2} \phi_m' \phi_n' + \kappa^2 \phi_m \phi_n \right) dz = \delta_{mn}. \quad (\text{A7})$$

The expression in terms of  $\phi_m$  and  $\phi_n$  is found by using (A6) and (9) to eliminate  $\xi_m, \xi_n$  and the eigenvalues, then integrating by parts, which removes boundary terms. Correspondingly,

$$\langle \xi_m, \mathcal{P}\xi_n \rangle = \frac{\mu_n^2}{H} \int_{z^-}^{z^+} \left( \frac{f^2}{N^2} \phi_m' \phi_n' + \kappa^2 \phi_m \phi_n \right) dz = \mu_n^2 \delta_{mn} \quad (\text{A8})$$

and

$$\begin{aligned} \langle \mathcal{P}^{-1} \mathcal{E}\xi_m, \mathcal{E}\xi_n \rangle &= \frac{1}{H} \int_{z^-}^{z^+} \phi_m \phi_n dz \\ &\quad + \frac{\phi_m(z^+) \phi_n(z^+)}{\alpha_+} + \frac{\phi_m(z^-) \phi_n(z^-)}{\alpha_-} \\ &= \mu_n^{-2} \delta_{mn}. \end{aligned} \quad (\text{A9})$$

The latter relation (A9) has the advantage of involving only the undifferentiated streamfunctions, while the first relation (A7) is independent of the eigenvalues and  $\alpha_\pm$ .

The basis of eigenfunctions can be used to project data: given  $\mathbf{Q}$  or  $\psi$ , we can write

$$\mathbf{Q} = \sum_n a_n \xi_n \quad (\text{A10})$$

and expand  $\psi$  as in (11). The amplitude coefficients  $a_n$  can be found using one of the orthogonality relations (A7) or (A8); the expression (12), for example, follows from (A7), since  $a_n = \langle \xi_n, \mathcal{E}\mathbf{Q} \rangle$ .

As mentioned at the end of section 2, our choice of orthogonality conditions implies unfamiliar dimensions for the eigenfunctions. Expanding on those comments, note that because  $[q], [b^\pm] \sim [T^{-1}]$  and  $[\mu] \sim [L^{-1}]$ , (A5) implies that  $[\xi] \sim [L^{-2}][\phi]$ . The orthogonality condition (10) demands  $[\phi] \sim [L]$  and therefore  $[\xi] \sim [L^{-1}]$ .

*c. Properties of the operators and eigenfunctions*

Here we prove a few relevant facts about the eigenvectors and eigenvalues of (A5). First, we show that

the operator  $\mathcal{E}$  is self-adjoint, for example,  $\langle \xi_m, \mathcal{E}\xi_n \rangle = \langle \mathcal{E}\xi_m, \xi_n \rangle$ . Expanding the left-hand side and integrating by parts, we find

$$\begin{aligned} \langle \xi_m, \mathcal{E}\xi_n \rangle &= \frac{1}{H} \int_{z^-}^{z^+} -\bar{\xi}_m \phi_n dz + \bar{\xi}_m^+ \phi_n(z^+) - \bar{\xi}_m^- \phi_n(z^-), \\ &= \frac{1}{H} \int_{z^-}^{z^+} -\phi_n \left( \frac{f^2}{N^2} \bar{\phi}_m' \right)' + \kappa^2 \bar{\phi}_m \phi_n dz + \frac{f^2}{HN^2(z^+)} \bar{\phi}_m'(z^+) \phi_n(z^+) - \frac{f^2}{HN^2(z^-)} \bar{\phi}_m'(z^-) \phi_n(z^-), \\ &= \frac{1}{H} \int_{z^-}^{z^+} \frac{f^2}{N^2} \phi_n' \bar{\phi}_m' + \kappa^2 \bar{\phi}_m \phi_n dz, \\ &= \langle \mathcal{E}\xi_m, \xi_n \rangle \end{aligned}$$

since the expression on the penultimate line is clearly symmetric. The self-adjointness of  $\mathcal{P}$  as well as the positive definiteness is obvious.

To establish the completeness of the basis of the eigenvector  $\xi_n$ , we rewrite the eigenvalue problem in the standard form  $\mathcal{A}\xi_n = \mu_n^{-2}\xi_n$ , where  $\mathcal{A} = \mathcal{P}^{-1}\mathcal{E}$  is positive definite and self-adjoint. This operator is compact when acting on the Hilbert space of vectors  $\mathbf{Q}$  with bounded norm  $\langle \mathbf{Q}, \mathbf{Q} \rangle$ . This is because it is essentially an integral operator with continuous kernel—the Green’s function of the operator  $(s\phi')' - \kappa^2\phi$  (e.g., Debnath and Mikusiński 1998, section 4.8). The Hilbert–Schmidt theorem (Debnath and Mikusiński 1998, section 4.10) then applies to guarantee that every vector  $\mathbf{Q}$  has a unique convergent expansion in terms of the  $\xi_n$ .

$\bar{\Delta\rho} = \rho_j - \rho_1$  is the average background density jump between levels,  $\rho_j = \rho(z_j)$  is the background density, and  $\rho_0$  is the average density. The parameter  $s = N_0^2/N^2$  is discretized as  $s_j = s(z_{j+1/2}) \equiv \bar{\Delta\rho}/(\rho_{j+1} - \rho_j)$ , thus  $s_j$  is offset by a half space from  $\rho_j$ . In this discretization, the SBs and PV are

$$\begin{aligned} b^+ &= \frac{f^2}{N_0^2 H} s\psi'|_{z=0} \rightarrow L_D^{-2} \frac{s_1}{\delta} (\psi_1 - \psi_2), \\ b^- &= \frac{f^2}{N_0^2 H} s\psi'|_{z=-1} \rightarrow L_D^{-2} \frac{s_{J-1}}{\delta} (\psi_{J-1} - \psi_J), \quad \text{and} \\ q &= \left( \frac{f^2}{N_0^2} s\psi' \right)' - \kappa^2 \psi \rightarrow L_D^{-2} \frac{1}{\delta^2} [s_{j-1}\psi_{j-1} - (s_{j-1} + s_j)\psi_j \\ &\quad + s_j\psi_{j+1}] - \kappa^2 \psi_j, \end{aligned}$$

APPENDIX B

**Discrete Eigenvalue Problem and Numerical Computation of Modes**

Here we construct the discrete version of the eigenvalue problem. Assuming a constant discrete coordinate  $z_j$  on  $J$  grid points, with  $z_1 = 0$  at the top,  $z_J = -H$  at the bottom, and a constant finite difference  $\Delta z = z_j - z_{j+1}$ , the mean stratification is  $N_0^2 = (g/\rho_0)\bar{\Delta\rho}/\Delta z$ , where

where  $\delta \equiv \Delta z/H$  and  $L_D \equiv N_0 H/f$ . Nondimensionalizing  $\kappa \mapsto [L_D^{-1}]\kappa$ ,  $\psi \mapsto [L_D^2 T^{-1}]\psi$  and  $(q, b^\pm) \mapsto [T^{-1}](q, b^\pm)$  (for some time scale  $T$ ), the discrete PV/SBs and streamfunction are related as

$$\mathbf{Q} = \mathbf{A}\psi,$$

where

$$\mathbf{A} = \frac{1}{\delta^2} \begin{bmatrix} \delta s_1 & -\delta s_1 & 0 & \dots & \dots & 0 \\ s_1 & -(s_1 + s_2 + \delta^2 \kappa^2) & s_2 & 0 & \dots & 0 \\ & & & & \dots & \\ 0 & \dots & 0 & s_{J-2} & -(s_{J-2} + s_{J-1} + \delta^2 \kappa^2) & s_{J-1} \\ 0 & \dots & & 0 & \delta s_{J-1} & -\delta s_{J-1} \end{bmatrix}. \quad (\text{B1})$$

Defining the operators

$$\mathbf{B} = \begin{pmatrix} 1 & 0 & \dots & 0 \\ 0 & \delta & \dots & 0 \\ 0 & \dots & \delta & 0 \\ 0 & \dots & 0 & 1 \end{pmatrix} \quad \text{and} \quad \mathbf{F} = \begin{pmatrix} 1 & 0 & \dots & 0 \\ 0 & -1 & \dots & 0 \\ 0 & \dots & 0 & -1 \end{pmatrix}, \quad (\text{B2})$$

one sees that  $\mathbf{B}$  plays the part of the inner product, for example,  $\langle \xi_1, \xi_2 \rangle \rightarrow \xi_1^T \mathbf{B} \xi_2$  and  $\mathbf{F}$  accomplishes the awkward sign changes in the definition of the operator  $\mathcal{E}$ . The energy in wavenumber  $\kappa$  is

$$E_\kappa = \frac{\delta}{2} \left[ \sum_{j=1}^{J-1} s_j \left| \frac{\psi_j - \psi_{j-1}}{\delta} \right|^2 + \kappa^2 \sum_{j=2}^{J-1} |\psi_j|^2 \right] = \frac{1}{2} \psi^* \mathbf{F} \mathbf{B} \mathcal{E} \psi.$$

For consistency with the theoretical development in section 2, we may also write the energy in terms of the vector  $\mathbf{Q} = \mathbf{A} \psi$ ,

$$E_\kappa = \frac{1}{2} \mathbf{Q}^* \mathbf{B} \mathbf{F} \mathbf{A}^{-1} \mathbf{Q} = \frac{1}{2} \mathbf{Q}^* \mathbf{B} \mathcal{E} \mathbf{Q}$$

where the symmetry of  $\mathbf{F}$  and  $\mathbf{B}$  were used, and  $\mathcal{E} \equiv \mathbf{F} \mathbf{A}^{-1}$  is defined to make the discrete version of the energy operator defined in (A3) perfectly clear.

Similarly, the generalized enstrophy in wavenumber  $\kappa$  is

$$P_\kappa = \frac{1}{2} \mathbf{Q}^* \mathbf{B} \mathcal{P} \mathbf{Q}$$

where we define

$$\mathcal{P} = \begin{pmatrix} \alpha_+ & 0 & \dots & 0 \\ 0 & 1 & \dots & 0 \\ 0 & \dots & 1 & 0 \\ 0 & \dots & 0 & \alpha_- \end{pmatrix}$$

to make clear the analogy with the generalized enstrophy operator defined in (A3).

Now note that  $\mathbf{B} \mathcal{E}$  and  $\mathbf{B} \mathcal{P}$  are both symmetric (the former can be verified by checking that  $\mathbf{F} \mathbf{B} \mathbf{A}$  is symmetric), so we can simultaneously diagonalize the two quadratic forms  $E_\kappa$  and  $P_\kappa$  by solving the generalized eigenvalue problem  $\mathbf{B} \mathcal{P} \xi_j = \mu_j^2 \mathbf{B} \mathcal{E} \xi_j$  or, in matrix form

$$(\mathbf{B} \mathcal{P}) \mathbf{X} = (\mathbf{B} \mathcal{E}) \mathbf{X} \mathbf{M}^2,$$

where  $\mathbf{X}$  is the matrix with columns  $\xi_j$  and  $\mathbf{M}^2$  has  $\mu_j^2$  along its diagonal and zeros elsewhere. Solutions to this generalized eigenvalue problem obey the orthogonality relations

$$\mathbf{X}^T \mathbf{B} \mathcal{E} \mathbf{X} = \mathbf{I} \quad \text{and} \quad \mathbf{X}^T \mathbf{B} \mathcal{P} \mathbf{X} = \mathbf{M}^2, \quad (\text{B3})$$

which are analogous to (10) and (A8), respectively.

In practice, it is more convenient to define a streamfunction eigenfunction  $\phi$  such that  $\mathbf{A} \phi = \xi$ , so that the generalized eigenvalue problem can be rewritten as  $\mathbf{F} \mathcal{P} \mathbf{A} \phi_j = \mu_j^2 \phi_j$ , or in matrix form

$$\mathbf{F} \mathcal{P} \mathbf{A} \Phi = \Phi \mathbf{M}^2, \quad (\text{B4})$$

where  $\Phi$  has  $\phi_j$  as its columns. In this case, the orthogonality relations become

$$\Phi^T \mathbf{F} \mathbf{B} \mathbf{A} \Phi = \mathbf{I} \quad \text{and} \quad \Phi^T \mathcal{P} \mathbf{B} \mathbf{A}^2 \Phi = \mathbf{M}^2, \quad (\text{B5})$$

where we have used the fact that  $\mathbf{F}^2 = \mathbf{I}$ . Finally, writing (B4) as  $\Phi^{-1} (\mathbf{A}^{-1} \mathcal{P}^{-1} \mathbf{F}) \Phi = \mathbf{M}^2$  and using the first relation in (B5), we have the equivalent of (A9),

$$\Phi^{-1} \mathbf{B} \mathcal{P}^{-1} \Phi = \mathbf{M}^{-2}. \quad (\text{B6})$$

The expansion in the basis of eigenvectors  $\phi_n$  of discrete data is readily expressed in terms of the matrix  $\Phi$ . Denoting by  $\psi$  the column vector of the streamfunction data (Fourier transformed in the horizontal)  $\psi(z_j)$ , the expansion reads

$$\psi = \Phi \mathbf{a}, \quad (\text{B7})$$

where  $\mathbf{a} = (a_1, \dots, a_J)^T$  is the column vector of the mode amplitudes. These amplitudes are obtained from the data using the relation

$$\mathbf{a} = \Phi^T \mathbf{F} \mathbf{B} \mathbf{A} \psi,$$

which is deduced from (B5) and (B7). The total energy at a given wavenumber  $\kappa$ ,

$$E_\kappa = \frac{1}{2} \psi^* \mathbf{F} \mathbf{B} \mathcal{E} \psi = \frac{1}{2} |\mathbf{a}|^2,$$

where  $*$  denotes the complex (conjugate) transpose, is clearly the sum of the individual contributions  $|a_n|^2/2$  of each mode. Similarly, the generalized enstrophy,

$$P_\kappa = \frac{1}{2} \mathbf{Q}^* \mathbf{B} \mathcal{P} \mathbf{Q} = \frac{1}{2} \psi^* \mathcal{P} \mathbf{B} \mathbf{A}^2 \psi = \frac{1}{2} \mathbf{a}^* \mathbf{M}^2 \mathbf{a},$$

is the sum of the contributions  $\mu_n^2 |a_n|^2/2$ .

## REFERENCES

- Blumen, W., 1982: Wave interactions in quasi-geostrophic uniform potential vorticity flow. *J. Atmos. Sci.*, **39**, 2388–2396.
- Bretherton, F. P., 1966: Critical layer instability in baroclinic flows. *Quart. J. Roy. Meteor. Soc.*, **92**, 325–334.
- Chelton, D. B., M. G. Schlax, and R. M. Samelson, 2011: Global observations of nonlinear mesoscale eddies. *Prog. Oceanogr.*, **91**, 167–216.
- Debnath, L., and P. Mikusiński, 1998: *Introduction to Hilbert Spaces*. 2nd ed. Academic Press, 551 pp.
- Fu, L.-L., and R. Ferrari, 2008: Observing oceanic submesoscale processes from space. *Eos, Trans. Amer. Geophys. Union*, **89**, 488, doi:10.1029/2008EO480003.
- Goldstein, H., 1980: *Classical Mechanics*. 2nd ed. Addison-Wesley, 638 pp.
- Held, I. M., R. T. Pierrehumbert, S. T. Garner, and K. L. Swanson, 1995: Surface quasi-geostrophic dynamics. *J. Fluid Mech.*, **282**, 1–20.
- Horn, R. A., and C. R. Johnson, 1990: *Matrix Analysis*. Cambridge University Press, 575 pp.
- Hua, B. L., and D. B. Haidvogel, 1986: Numerical simulations of the vertical structure of quasi-geostrophic turbulence. *J. Atmos. Sci.*, **43**, 2923–2936.
- Isern-Fontanet, J., B. Chapron, G. Lapeyre, and P. Klein, 2006: Potential use of microwave sea surface temperatures for the estimation of ocean currents. *Geophys. Res. Lett.*, **33**, L24608, doi:10.1029/2006GL027801.
- , G. Lapeyre, P. Klein, B. Chapron, and M. W. Hecht, 2008: Three-dimensional reconstruction of oceanic mesoscale currents from surface information. *J. Geophys. Res.*, **113**, C09005, doi:10.1029/2007JC004692.
- Klein, P., B. L. Hua, G. Lapeyre, X. Capet, S. L. Gentil, and H. Sasaki, 2008: Upper-ocean turbulence from high resolution 3D simulations. *J. Phys. Oceanogr.*, **38**, 1748–1763.
- LaCasce, J. H., and A. Mahadevan, 2006: Estimating subsurface horizontal and vertical velocities from sea surface temperature. *J. Mar. Res.*, **64**, 695–721.
- Lapeyre, G., 2009: What mesoscale signal does the altimeter reflect? On the decomposition in baroclinic modes and a surface-trapped mode. *J. Phys. Oceanogr.*, **39**, 2857–2874.
- , and P. Klein, 2006: Dynamics of the upper oceanic layers in terms of surface quasigeostrophy theory. *J. Phys. Oceanogr.*, **36**, 165–176.
- Le Traon, P. Y., P. Klein, and B. L. Hua, 2008: Do altimeter wavenumber spectra agree with the interior or surface quasigeostrophic theory? *J. Phys. Oceanogr.*, **38**, 1137–1142.
- Ripa, P., 2001: Waves and resonance in free-boundary baroclinic instability. *J. Fluid Mech.*, **428**, 387–408.
- Scott, R. B., and D. G. Furnival, 2012: Assessment of traditional and new eigenfunction bases applied to extrapolation of surface geostrophic current time series to below the surface in an idealized primitive equation simulation. *J. Phys. Oceanogr.*, **42**, 165–178.
- Smith, K. S., and R. Ferrari, 2009: The production and dissipation of compensated thermohaline variance by mesoscale stirring. *J. Phys. Oceanogr.*, **39**, 2477–2501.
- , G. Boccaletti, C. C. Henning, I. N. Marinov, C. Y. Tam, I. M. Held, and G. K. Vallis, 2002: Turbulent diffusion in the geostrophic inverse cascade. *J. Fluid Mech.*, **469**, 13–48.
- Stammer, D., 1997: Global characteristics of ocean variability estimated from regional TOPEX/Poseidon altimeter measurements. *J. Phys. Oceanogr.*, **27**, 1743–1769.
- Tulloch, R. T., and K. S. Smith, 2009: Quasigeostrophic turbulence with explicit surface dynamics: Application to the atmospheric energy spectrum. *J. Atmos. Sci.*, **66**, 450–467.
- Wunsch, C., 1997: The vertical partition of oceanic horizontal kinetic energy. *J. Phys. Oceanogr.*, **27**, 1770–1794.